Characterization and Modeling of Charge Trapping: From Single Defects to Devices

T. Grasser[1], G. Rzepa[1], M. Waltl[1], W. Goes[1], K. Rott[2], G. Rott[2], H. Reisinger[2], J. Franco[3], and B. Kaczer[3]

[1]*Institute for Microelectronics, TU Wien, Austria* [2]*Infineon, Munich, Germany* [3]*imec, Belgium*

Abstract

Using time-dependent defect spectroscopy measurements on nanoscale MOSFETs, individual defects have been characterized in much greater detail than ever before. These studies have revealed the existence of metastable defect states which have a significant impact on the capture and emission time constants. For example, these defect states explain the large emission time constants observed in bias temperature measurements as well as the switching behavior of defects sensitive to gate bias changes towards accumulation. By carefully analyzing the properties of the defects contributing to random telegraph noise and the recoverable component of the bias temperature instability, it could be confirmed that both phenomena are due to the same type of defect. The most fundamental property of these defects is that their time constants are widely distributed, leading to the ubiquitous time and frequency dependence. By transferring this knowledge to large area devices, noise as well as the response to bias temperature stress and recovery can be understood in great detail.

1. Introduction

Charge trapping has been considered an essential contributor to semiconductor device reliability starting from the earliest technologies. In particular, it has been made responsible for random telegraph noise (RTN) [1–5] and recently been identified as a significant contributor to bias temperature instabilities (BTI) [6–12]. Consistent with detailed NBTI studies [13, 14], the individual defects visible in RTN and time-dependent defect spectroscopy (TDDS) show a very wide distribution of time constants. Unfortunately, TDDS studies are very time consuming and thus not too well suited for the study of these distributions [15]. While missing some details, the wide distributions of the effective time constants can be extracted from large-area devices and represented in capture/emission time (CET) maps [16–18]. These CET maps show some interesting bias and temperature dependencies which can be linked back to the TDDS-based trap models. This allows us to establish a link between RTN and BTI [19], with the recoverable component of BTI being the non-equilibrium response of the same traps causing RTN. We summarize the recent advances, showing how the degradation in large-area devices can be understood as the collective response of a large number of individual defects.

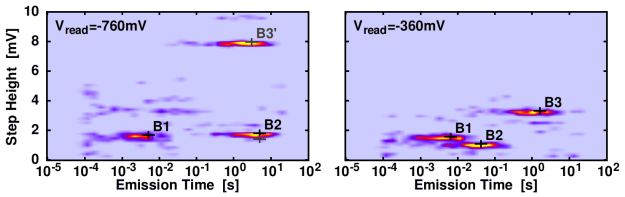

Fig. 1. Typical spectral maps obtained by the TDDS at two different readout (recovery) voltages. Three defects are clearly visible. Defect B1, is a fixed charge trap with an emission time independent of the readout voltage. Defects B2 and B3, however, are switching oxide traps with a bias-dependent emission time, with B2 being much more sensitive than B3. Also, for these defects, the step-heights are very sensitive to the readout voltage [20].

2. Individual Defects – Experimental

For our experimental assessment we have made extensive use of TDDS [21], which allow for BTI studies on small-area devices at the single-defect level [8, 22–24]. Since such devices contain only a countable number of defects, the recovery of each defect is visible as a discrete step in the recovery trace. Typically, the heights of these discrete steps are exponentially distributed [20, 25], just as those in RTN studies [26, 27]. In a TDDS setup, a nanoscale device is repeatedly stressed and recovered (say $N = 100$ times) using fixed stress/recovery times. The recovery trace is analyzed for discrete steps of height η occurring at a certain time τ_e. Each (τ_e, η) pair is then placed into a 2D histogram, which we call the spectral map, see Fig. 1. The clusters forming in the spectral maps reveal the probability density distribution and thus provide detailed information on the statistical nature of the average trap annealing time constant $\bar{\tau}_e$. From the evolution of the spectral map as a function of stress time, the average capture time $\bar{\tau}_c$ can be extracted as well. All observed distributions for τ_e and τ_c were found to be exponential, consistent with simple first-order processes [2, 15, 28] but inconsistent with the traditional reaction-diffusion formalism [29–31].

3. Individual Defects – Modeling

Based on the extended TDDS data, a clear picture of the defect dynamics has emerged, which required us to go beyond the traditional two-state description [21, 24, 28, 32], see Fig. 2. Notable features include the uncorrelated capture and emission times, the fact that about 50% of the traps are sensitive to the readout voltage (switching traps), while the others are not (fixed charge traps), and

978-1-4799-2153-9/14/$31.00 ©2014 IEEE

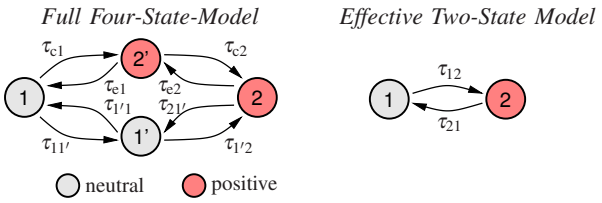

Fig. 2. **Left**: The four states of oxide defects extracted from TDDS experiments [21]. Each defect has two stable states, 1 and 2, and possibly two metastable states 1' and 2'. The metastable state 2' seems to be always present, while the existence of the metastable state 1' decides on whether the trap behaves like a fixed positive or a switching trap [36, 37]. **Right**: An effective two-state approximation of the four-state defect using the first-passage times τ_{12} and τ_{21} [21, 28].

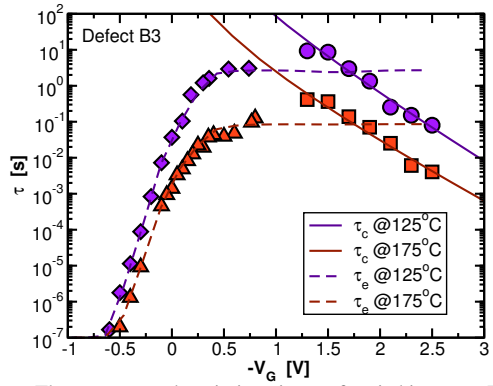

Fig. 3. The capture and emission times of switching trap B3 at two temperatures (symbols: data, lines: four-state NMP model). Excellent agreement is obtained over 8 orders of magnitude.

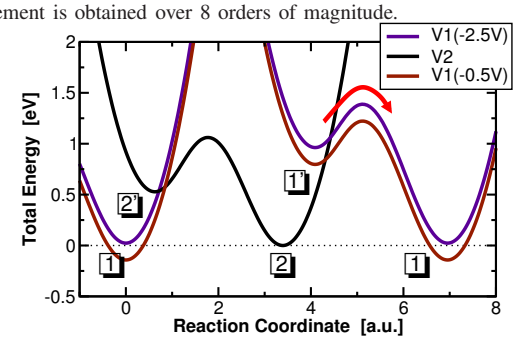

Fig. 4. CC diagram for the switching trap B3. Contrary to defect B1, the metastable state 1' is accessible, leading to strongly bias-dependent recovery via the sequence 2→1'→1 at more positive gate bias.

a pronounced frequency dependence [33]. Charge state transitions are modeled using nonradiative multiphonon (NMP) theory [34, 35], while the others are assumed to follow simple transition state theory. Excellent agreement with experimental data has been obtained for both fixed charge traps (not shown here, see e.g. [24]), and switching oxide traps, see Fig. 3. Except for the depth of the trap in the oxide, the dynamics of the transitions are completely determined by the configuration coordinate (CC) diagram, giving the potential energy surface in the Born-Oppenheimer approximation (see Fig. 4).

4. The Wide Distributions: Large-Area Devices

All capture and emission events observed using TDDS were exponentially distributed [15, 24], consistent with

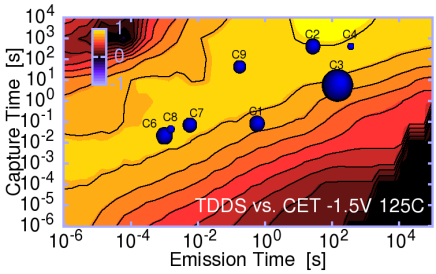

Fig. 5. The extracted values of τ_c^H and τ_e^L shown against a CET map extracted from the same technology [18], which is fully consistent with this particular configuration observed by TDDS in device C. The size of the dots is given by B_i, the maximum impact on ΔV_{th}.

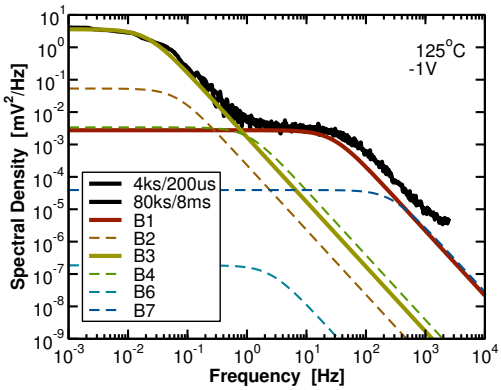

Fig. 6. The experimental power spectral density (black lines) is dominated by the defects B1 and B3. Other contributions to the PSD are negligible in the frequency range 1 mHz - 1 kHz.

first-order processes. As has been shown [21, 32], the four-state defect model of Fig. 2 can be well approximated by such a first-order process, at least under quasi-DC stress conditions. To the first order, the response of the defects to BTI stress can therefore be approximated by the familiar exponential transitions between the equilibrium configurations. As an example, we consider a switch of the gate bias between a low (V_G^L) and a high voltage (V_G^H). Keeping in mind the stochastic nature of these transitions, we have for the expectation value of the threshold voltage shift $\Delta V_{th} = \sum B_i(1-\exp(-t_s/\tau_{c,i}^H))\exp(-t_r/\tau_{e,i}^L)$ for all stress and recovery times (t_s and t_r) with $B_i = \eta_i \tau_{e,i}^H/(\tau_{e,i}^H + \tau_{c,i}^H)$. For large-area devices, the sum can be converted to an integral over a distribution of capture and emission times, the so-called capture/emission time (CET) map. By inverting this relation, the CET map can be directly extracted from experimental data by taking the second-order mixed derivative [16, 28]. Such a CET map is shown in Fig. 5 together with a few individual defects extracted by TDDS for a device of the same technology.

5. The Link between RTN and BTI

By extracting $\bar{\tau}_c(V_G)$ and $\bar{\tau}_e(V_G)$ of all defects contributing to BTI recovery in a selected nano-scale device, their stochastic response to various changes in the bias conditions can be predicted. In particular, their typical

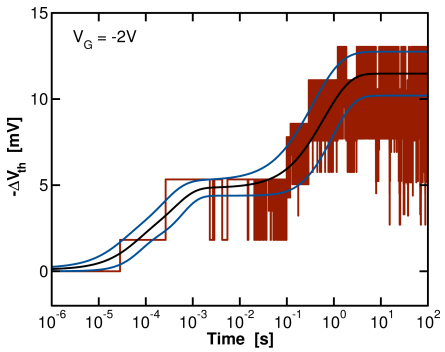

Fig. 7. If the bias dependence of the capture and emission times is known, the stochastic response of the defects to BTI conditions can be understood. Shown is a single realization of the stochastic process (red lines), together with the mean ΔV_{th} (black) and the $\pm\sigma$ values (blue).

equilibrium response to a constant V_{G} will be RTN, even though the capture times can become extremely large at lower gate biases, e.g. 10 ks [19]. The correctness of this assertion has been checked at various bias conditions and temperatures, as shown for instance in Fig. 6, where the TDDS defects correctly reproduce the experimentally recorded power spectral density (PSD).

Subjected to varying gate biases, the defects will go from one equilibrium into another, resulting in stochastic BTI, see Fig. 7. It can be seen that particularly for operating-bias conditions, a considerable amount of noise is produced in this process, which is not modeled when only the conventional mean values are studied.

6. Physics-Based Reliability Modeling

In order to understand the physics behind the CET maps, we use the four-state NMP model for the oxide traps and a simple double-well model for the quasi-permanent interface traps to describe the response of large-area devices subjected to various stress and recovery conditions [38]. The parameters describing the CC diagrams are assumed to be independent and normally distributed, see Fig. 8, and calibrated to experimental data, see Fig. 9, resulting in excellent agreement. Based on this calibration, CET maps can be calculated and compared to experimental values, see Fig. 10 and Fig. 11, where good agreement with the data is observed.

7. Conclusions

Based on a detailed defect model extracted using TDDS, we have developed a four-state model for oxide traps. This model can be used to study RTN and BTI in nano-scale and large-area devices, where for BTI also a contribution from more permanent defects, likely interface states, has to be added. Creation and annealing of these quasi-permanent defects is also consistent with a first-order process. Using this model, lifetime predictions taking the stochastic nature of the degradation into account are possible for arbitrary stress-recovery sequences.

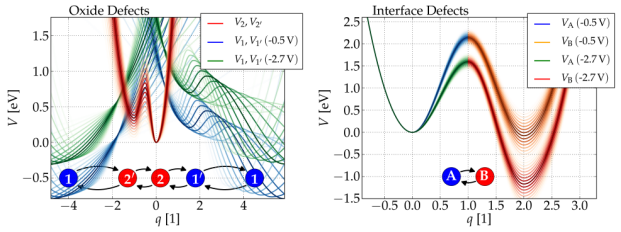

Fig. 8. The extracted distribution of the CC diagrams. The opaque lines represent the mean values and the fade-out illustrates up to one σ of the distributions for $V_{\text{G}} = -0.5$ and -2.7 V. **Left**: The NMP four-state model with an exemplary interface distance $x_{\text{t}} = 0.6$ nm (states 1 and 1' neutral, states 2 and 2' positive). **Right**: The double well model for simulation of interface defects. Once in state B, the charge state is determined using an amphoteric SRH model [39].

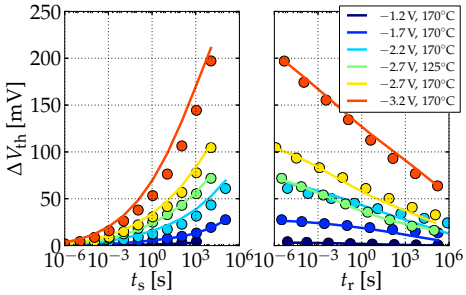

Fig. 9. Comparison of simulated threshold voltage shifts (solid lines) to the experimental data (dots) during stress (t_{s}) and recovery (t_{r}) for different temperature and gate voltage combinations.

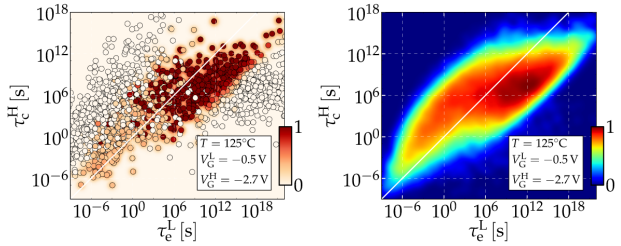

Fig. 10. CET map computed from individual defects with capture time constants $\tau_{\text{c}}^{\text{H}}$ during stress (V_{G}^{H}) and emission time constants $\tau_{\text{e}}^{\text{L}}$ during recovery (V_{G}^{L}). **Left**: Randomly selected oxide and interface defects. Their color indicates their equilibrium occupancy difference. **Right**: CET map calculated from the simulation result using all defects.

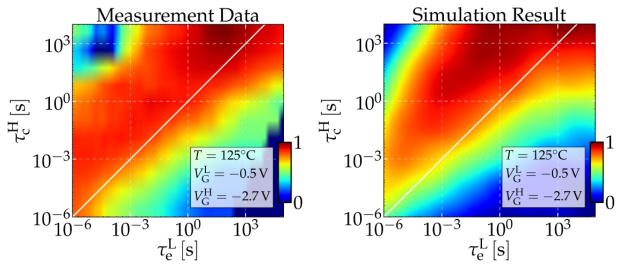

Fig. 11. Comparison of the measured (**left**) and simulated (**right**) CET maps. As expected, the important characteristics are reproduced: the center of the distribution is above the $\tau_{\text{c}} = \tau_{\text{e}}$ axis for lower emission times and starts to cross the axis for higher emission times.

Acknowledgments: The research leading to these results has received funding from the FWF project n°23390-M24, the European Community's FP7 project n°261868 (MORDRED), and the Intel Sponsored Research Project n° 2013111914.

References

[1] K. Ralls, W. Skocpol, L. Jackel, R. Howard, L. Fetter, R. Epworth, and D. Tennant, "Discrete Resistance Switching in Submicrometer Silicon Inversion Layers: Individual Interface Traps and Low-Frequency ($1/f$?) Noise," *Phys.Rev.Lett.*, vol. 52, no. 3, pp. 228–231, 1984.

[2] M. Kirton and M. Uren, "Noise in Solid-State Microstructures: A New Perspective on Individual Defects, Interface States and Low-Frequency (1/f) Noise," *Adv.Phys.*, vol. 38, no. 4, pp. 367–486, 1989.

[3] A. Palma, A. Godoy, J. A. Jimenez-Tejada, J. E. Carceller, and J. A. Lopez-Villanueva, "Quantum Two-Dimensional Calculation of Time Constants of Random Telegraph Signals in Metal-Oxide-Semiconductor Structures," *Phys.Rev.B*, vol. 56, no. 15, pp. 9565–9574, 1997.

[4] D. Fleetwood, H. Xiong, Z.-Y. Lu, C. Nicklaw, J. Felix, R. Schrimpf, and S. Pantelides, "Unified Model of Hole Trapping, $1/f$ Noise, and Thermally Stimulated Current in MOS Devices," *IEEE Trans.Electr.Dev.*, vol. 49, no. 6, pp. 2674–2683, 2002.

[5] T. Nagumo, K. Takeuchi, T. Hase, and Y. Hayashi, "Statistical Characterization of Trap Position, Energy, Amplitude and Time Constants by RTN Measurement of Multiple Individual Traps," in *Proc. IEDM*, 2010, pp. 628–631.

[6] C. Zhao, J. Zhang, G. Groeseneken, and R. Degraeve, "Hole-Traps in Silicon Dioxides - Part II: Generation Mechanism," *IEEE Trans.Electr.Dev.*, vol. 51, no. 8, pp. 1274–1280, 2004.

[7] V. Huard, C. Parthasarathy, and M. Denais, "Single-Hole Detrapping Events in pMOSFETs NBTI Degradation," in *IIRW Final Rep.*, 2005, pp. 5–9.

[8] T. Wang, C.-T. Chan, C.-J. Tang, C.-W. Tsai, H. Wang, M.-H. Chi, and D. Tang, "A Novel Transient Characterization Technique to Investigate Trap Properties in HfSiON Gate Dielectric MOSFETs-From Single Electron Emission to PBTI Recovery Transient," *IEEE Trans.Electr.Dev.*, vol. 53, no. 5, pp. 1073–1079, 2006.

[9] D. Ang, S. Wang, G. Du, and Y. Hu, "A Consistent Deep-Level Hole Trapping Model for Negative Bias Temperature Instability," *IEEE Trans.Dev.Mat.Rel.*, vol. 8, no. 1, pp. 22–34, 2008.

[10] T. Grasser, B. Kaczer, W. Goes, T. Aichinger, P. Hehenberger, and M. Nelhiebel, "Understanding Negative Bias Temperature Instability in the Context of Hole Trapping," *Microelectr.Eng.*, vol. 86, no. 7-9, pp. 1876–1882, 2009.

[11] H. Reisinger, T. Grasser, and C. Schlünder, "A Study of NBTI by the Statistical Analysis of the Properties of Individual Defects in pMOSFETs," in *IIRW Final Rep.*, 2009, pp. 30–35.

[12] T. Grasser, Ed., *Bias Temperature Instability for Devices and Circuits*. Springer, New York, 2014.

[13] B. Kaczer, T. Grasser, J. Martin-Martinez, E. Simoen, M. Aoulaiche, P. Roussel, and G. Groeseneken, "NBTI from the Perspective of Defect States with Widely Distributed Time Scales," in *Proc. IRPS*, 2009, pp. 55–60.

[14] M. Toledano-Luque, B. Kaczer, J. Franco, P. Roussel, T. Grasser, T. Hoffmann, and G. Groeseneken, "From Mean Values to Distributions of BTI Lifetime of Deeply Scaled FETs Through Atomistic Understanding of the Degradation," in *Proc. VLSI Symp.*, 2011.

[15] T. Grasser, K. Rott, H. Reisinger, M. Waltl, P. Wagner, F. Schanovsky, W. Goes, G. Pobegen, and B. Kaczer, "Hydrogen-Related Volatile Defects as the Possible Cause for the Recoverable Component of NBTI," in *Proc. IEDM*, Dec. 2013.

[16] H. Reisinger, T. Grasser, W. Gustin, and C. Schlünder, "The Statistical Analysis of Individual Defects Constituting NBTI and its Implications for Modeling DC- and AC-Stress," in *Proc. IRPS*, May 2010, pp. 7–15.

[17] H. Reisinger, T. Grasser, K. Ermisch, H. Nielen, W. Gustin, and C. Schlünder, "Understanding and Modeling AC BTI," in *Proc. IRPS*, Apr. 2011, pp. 597–604.

[18] T. Grasser, P.-J. Wagner, H. Reisinger, T. Aichinger, G. Pobegen, M. Nelhiebel, and B. Kaczer, "Analytic Modeling of the Bias Temperature Instability Using Capture/Emission Time Maps," in *Proc. IEDM*, Dec. 2011, pp. 27.4.1–27.4.4.

[19] T. Grasser, K. Rott, H. Reisinger, M. Waltl, J. Franco, and B. Kaczer, "A Unified Perspective of RTN and BTI," in *Proc. IRPS*, June 2014, pp. 4A.5.1–4A.5.7.

[20] J. Franco, B. Kaczer, M. Toledano-Luque, P. Roussel, J. Mitard, L. Ragnarsson, L. Witters, T. Chiarella, M. Togo, N. Horiguchi, G. Groeseneken, M. Bukhori, T. Grasser, and A. Asenov, "Impact of Single Charged Gate Oxide Defects on the Performance and Scaling of Nanoscaled FETs," in *Proc. IRPS*, 2012, p. 5A.4.1.

[21] T. Grasser, H. Reisinger, P.-J. Wagner, W. Goes, F. Schanovsky, and B. Kaczer, "The Time Dependent Defect Spectroscopy (TDDS) for the Characterization of the Bias Temperature Instability," in *Proc. IRPS*, May 2010, pp. 16–25.

[22] M. Toledano-Luque, B. Kaczer, P. Roussel, T. Grasser, G. Wirth, J. Franco, C. Vrancken, N. Horiguchi, and G. Groeseneken, "Response of a Single Trap to AC Negative Bias Temperature Stress," in *Proc. IRPS*, 2011, pp. 364–371.

[23] J. Zou, R. Wang, N. Gong, R. Huang, X. Xu, J. Ou, C. Liu, J. Wang, J. Liu, J. Wu, S. Yu, P. Ren, H. Wu, S. Lee, and Y. Wang, "New Insights into AC RTN in Scaled High-κ/Metal-gate MOSFETs under Digital Circuit Operations," in *Proc. VLSI Symp.*, 2012, pp. 139–140.

[24] T. Grasser, K. Rott, H. Reisinger, P.-J. Wagner, W. Goes, F. Schanovsky, M. Waltl, M. Toledano-Luque, and B. Kaczer, "Advanced Characterization of Oxide Traps: The Dynamic Time-Dependent Defect Spectroscopy," in *Proc. IRPS*, Apr. 2013, pp. 2D.2.1–2D.2.7.

[25] B. Kaczer, T. Grasser, P. Roussel, J. Franco, R. Degraeve, L. Ragnarsson, E. Simoen, G. Groeseneken, and H. Reisinger, "Origin of NBTI Variability in Deeply Scaled PFETs," in *Proc. IRPS*, 2010, pp. 26–32.

[26] A. Asenov, R. Balasubramaniam, A. Brown, and J. Davies, "RTS Amplitudes in Decananometer MOSFETs: 3-D Simulation Study," *IEEE Trans.Electr.Dev.*, vol. 50, no. 3, pp. 839–845, 2003.

[27] S. Amoroso, L. Gerrer, F. Adamu-Lema, S. Markov, and A. Asenov, "Statistical Study of Bias Temperature Instabilities by Means of 3D "Atomistic" Simulation," in *Bias Temperature Instability for Devices and Circuits*, T. Grasser, Ed. Springer, New York, 2014, pp. 323–348.

[28] T. Grasser, "Stochastic Charge Trapping in Oxides: From Random Telegraph Noise to Bias Temperature Instabilities," *Microelectr.Reliab.*, vol. 52, pp. 39–70, 2012.

[29] K. Jeppson and C. Svensson, "Negative Bias Stress of MOS Devices at High Electric Fields and Degradation of MNOS Devices," *J.Appl.Phys.*, vol. 48, no. 5, pp. 2004–2014, 1977.

[30] S. Mahapatra, N. Goel, S. Desai, S. Gupta, B. Jose, S. Mukhopadhyay, K. Joshi, A. Jain, A. Islam, and M. Alam, "A Comparative Study of Different Physics-Based NBTI Models," *IEEE Trans.Electr.Dev.*, vol. 60, no. 3, pp. 901–916, 2013.

[31] N. Goel, K. Joshi, S. Mukhopadhyay, N. Nanaware, and S. Mahapatra, "A comprehensive modeling framework for gate stack process dependence of DC and AC NBTI in SiON and HKMG p-MOSFETs," *Microelectr.Reliab.*, pp. xxx–xxx, 2014.

[32] W. Goes, F. Schanovsky, and T. Grasser, "Advanced Modeling of Oxide Defects," in *Bias Temperature Instability for Devices and Circuits*, T. Grasser, Ed. Springer, New York, 2014, pp. 409–446.

[33] T. Grasser, H. Reisinger, K. Rott, M. Toledano-Luque, and B. Kaczer, "On the Microscopic Origin of the Frequency Dependence of Hole Trapping in pMOSFETs," in *Proc. IEDM*, Dec. 2012, pp. 19.6.1–19.6.4.

[34] K. Huang and A. Rhys, "Theory of Light Absorption and Non-Radiative Transitions in F-Centres," *Proc.R.Soc.A*, vol. 204, pp. 406–423, 1950.

[35] D. Lang and C. Henry, "Nonradiative Recombination at Deep Levels in GaAs and GaP by Lattice-Relaxation Multiphonon Emission," *Phys.Rev.Lett.*, vol. 35, no. 22, pp. 1525–1528, 1975.

[36] A. Lelis and T. Oldham, "Time Dependence of Switching Oxide Traps," *IEEE Trans.Nucl.Sci.*, vol. 41, no. 6, pp. 1835–1843, Dec 1994.

[37] J. Conley Jr., P. Lenahan, A. Lelis, and T. Oldham, "Electron Spin Resonance Evidence that E'_γ Centers can Behave as Switching Oxide Traps," *IEEE Trans.Nucl.Sci.*, vol. 42, no. 6, pp. 1744–1749, 1995.

[38] T. Aichinger, M. Nelhiebel, and T. Grasser, "Unambiguous Identification of the NBTI Recovery Mechanism using Ultra-Fast Temperature Changes," in *Proc. IRPS*, 2009, pp. 2–7.

[39] Y. Yang and M. White, "Charge Retention of Scaled SONOS Nonvolatile Memory Devices at Elevated Temperatures," *Solid-State Electron.*, vol. 44, pp. 949–958, 2000.